Crimson Publishers
Wings to the Research

Review Article

Phase Distribution Evolution Mechanism During Horizontal-Vertical Flow Transition Process in Gas-Liquid Two-Phase Flow

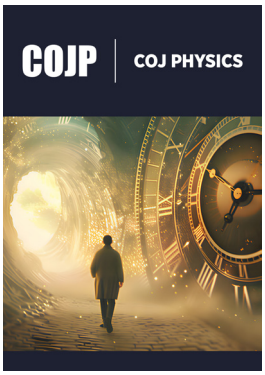

Nan Qu* and Zongrui Su

School of Energy and Environmental Engineering, University of Science and Technology Beijing, China

***Corresponding author:** Nan Qu, School of Energy and Environmental Engineering, University of Science and Technology Beijing, China

Submission: March 30, 2026
Published: May 15, 2026

Volume 1 - Issue 1

How to cite this article: Nan Qu* and Zongrui Su. Phase Distribution Evolution Mechanism During Horizontal-Vertical Flow Transition Process in Gas-Liquid Two-Phase Flow. COJ Phys. 1(1). COJP. 000501. 2026.
DOI: 10.31031/COJP.2026.01.000501

Abstract

This study investigates the phase distribution evolution mechanism of gas-liquid two-phase slug flow during the horizontal-to-vertical upward transition in a conventional 90-degree equal-diameter elbow using three-dimensional numerical simulation. The Volume of Fluid (VOF) model coupled with the standard k-ε turbulence model was employed to capture the dynamic gas-liquid interface. The validated model examined the flow pattern transition, the "nucleation-necking-detachment" process of bubble formation, and determined the minimum vertical pipe length required for the slug flow to achieve a fully developed state. The results show that under the combined action of centrifugal force, viscous drag, and surface tension within the elbow, the initial horizontal stratified flow transitions into vertical slug flow. A stable slug flow regime is established when Taylor bubbles exhibit a characteristic bullet shape with a conical head and a flattened tail, and their diameter approaches the pipe inner diameter. For the simulated configuration (pipe inner diameter D=25mm, elbow curvature radius R=5D), the minimum length required in the vertical pipe section is approximately 84.8D (2.12m). The calculated Taylor bubble rising velocity (1.0222m/s) at this developed state agrees closely with the theoretical value (0.98925m/s) from empirical correlations, with an error of about 3.33%. The findings indicate that a straight vertical segment of at least 85D downstream of a conventional 90-degree elbow is necessary to ensure stable, fully developed slug flow. This work provides a theoretical basis for optimizing pipeline layouts involving flow direction changes, particularly for applications like thermal diffusivity flow measurement which requires fully developed slug flow conditions.

Keywords: Slug flow; Horizontal-vertical transition; Phase distribution evolution; Numerical simulation; Minimum development length

Introduction

Gas-liquid two-phase flow, a complex flow state involving coexistence of gas and liquid phases, is widely prevalent in industrial sectors such as petroleum [1] and chemical engineering [2,3]. Accurate flow measurement is critical for process optimization and production safety. Current online non-displacement measurement methods include differential pressure [4], acoustic [5], and radiation techniques [6]. Among these, thermal diffusivity methods demonstrate significant application potential due to their non-contact and radiation-free advantages, though they require measurement under fully developed slug flow conditions. In oil and gas extraction, crude oil containing associated gas is commonly transported through pipelines using elbows to alter flow direction. However, when gas-liquid two-phase flow passes through elbows, centrifugal effects, interfacial tension, and gravity can lead to uneven wall pressure distribution and secondary flow [7], destabilizing downstream fluid distribution and flow characteristics, thereby compromising flow measurement accuracy. To ensure adequate development of gas-liquid two-phase flow, downstream elbow sections require extended

straight pipe segments for stable flow. For instance, when installing new thermal diffusivity flowmeters in horizontal pipes at onshore oilfield wellheads, approximately 100D (where D represents vertical pipe diameter) of vertical pipe is required to facilitate complete slug flow development [8]. However, excessive pipe length increases spatial requirements, compromising system compactness and flexibility. Installation methods and cost factors thus become critical considerations for engineering implementation.

As a common flow pattern in gas-liquid two-phase systems, slug flow exhibits discontinuous plug-like behavior between gas and liquid phases, characterized by pronounced intermittency and instability. As shown in Figure 1, the slug flow structure within a vertical circular pipe consists of gas plugs and liquid plugs [9]. Gas plugs occupy nearly the entire pipe cross-section with elliptical or parabolic front edges, while continuous liquid films form at the outer edges adjacent to the pipe wall. Liquid plugs located between adjacent gas plugs contain numerous microbubbles and move upward with relative velocity to the gas plugs. Flow parameters demonstrate periodic or non-periodic oscillations, with flow dynamics influenced by fluid properties, pipe geometry and dimensions. During underdeveloped stages, unstable gas-liquid flow results in irregular fluid distribution due to gas-liquid interactions between plugs. Taylor bubble tails form downward-moving liquid films that create jet structures converging into rear liquid plugs, disrupting adjacent plug motion. Experimental studies by Talvy et al. [10] revealed that when the distance between adjacent plugs is less than 3D, trailing Taylor bubbles exhibit significantly higher velocities than leading ones, predisposing to merging phenomena. When liquid plug tail velocities stabilize and adjacent Taylor bubble ascent rates align, slug flow reaches fully developed characteristics: regularized flow patterns with consistent bubble/liquid plug velocities, lengths, and phase interface distributions, where Taylor bubble diameters approximate pipe inner diameters. Academic consensus remains elusive regarding the minimum stable liquid plug length. Szalinski et al. [11] identified fully developed slug flow in vertical pipes at inlet heights exceeding 60-100D and 40D, respectively, while Saidj et al. [8] proposed a critical distance of 95D (Figure 1).

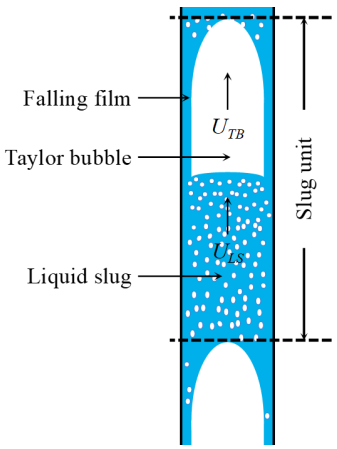

Figure 1: Diagram of gas-liquid slug flow structure in a vertical upward flow pipe.

The secondary flow within 90-degree bends alters phase interface distribution, leading to flow pattern changes. Its flow characteristics are influenced by multiple factors including gas holdup, gas and liquid phase apparent velocities, pipe diameter, bend arrangement, and gravity. Hsu et al. [12] observed that during horizontal-to-vertical upward flow, liquid phase in single bends generates significant vortex and counter-current phenomena with increasing pipe diameter. Han et al. [13] explained the mechanism of secondary swirling in 90-degree bends through numerical simulations: gas-liquid two-phase flow exhibits correlation between gas holdup and flow pattern evolution. Bubble flow transitions into elongated slug flow after passing through 90-degree bends, showing reduced cross-sectional gas holdup with periodic pulsation characteristics. Meanwhile, slug flow, agitated flow and annular flow evolve into stratified-wave flow with smaller gas holdup fluctuations.

To determine whether elastic flow in vertical pipes has fully developed, researchers can observe bubble coalescence and reference stable plug length studies, while also comparing experimental bubble velocities with empirical relationship calculations. Taylor bubble rising velocity in moving fluids approximates the sum of the maximum tube-wall boundary flow velocity (UTB) and bubble rising velocity in static media, expressed as $U_{TB} = U_l + U_0$.

Where, U_0 represents bubble drift velocity (m/s), Ul denotes fluid apparent velocity (m/s), and C is the fluid velocity influence coefficient on elastic flow bubble movement velocity. For fully developed laminar and turbulent flows, C values are 2.0 and 1.2 respectively.

$$U_o = 0.328\sqrt{\frac{gD(\rho_l - \rho_g)}{\rho_l}}$$

When the effects of viscosity and surface tension are neglected, U_0 can be expressed in the following analytical form: where g is the gravitational acceleration (m/s), D is the inner diameter of the pipeline (m), ρ_l is the liquid phase density at a given pressure and temperature (kg/m^3), and ρ_g is the gas phase density at the same conditions (kg/m^3).

Although research has been conducted on parameter characterization of gas-liquid two-phase flow, slug flow characteristics, and bend flow behavior, systematic studies on how different horizontal-vertical pipe connection configurations (e.g., bend angles and curvature radii) influence phase distribution evolution during flow pattern transition remain insufficient. Particularly, in-depth exploration of their impact on slug flow development in vertical pipes is still lacking.

This study employs numerical simulation methods to establish gas-liquid slug flow models under various horizontal-vertical pipe connection configurations. By solving key parameters including flow velocity, pressure and phase distribution, we analyze flow pattern transitions, bubble coalescence and breakup phenomena during flow direction changes, and investigate the mechanisms by which connection structures affect phase distribution and flow characteristics. The research aims to identify optimal connection

configurations that facilitate rapid attainment of fully developed slug flow in vertical pipes, providing theoretical foundations and practical guidance for industrial pipeline system optimization and flow measurement technology improvements.

Numerical Simulation Methods

Geometric models and meshing

Physical model: To investigate phase distribution characteristics of gas-liquid two-phase flow during flow direction transition, this study adopts a 90-degree equal-diameter elbow as design condition, as illustrated in Figure 2. Physical models consist of cylindrical pipes comprising horizontal sections, elbow zones, and vertical pipes. Gas-liquid two-phase flow enters through horizontal pipe inlets, undergoes directional change via the connection structure, and exits through vertical riser outlets. To ensure consistent experimental variables for elastic flow development, all configurations maintain uniform horizontal pipe dimensions with an inner diameter D1 of 25mm and length y of 1.5m ($60D_1$), enabling stable flow characteristics of gas-liquid two-phase flow in horizontal pipes prior to elbow entry (Figure 2).

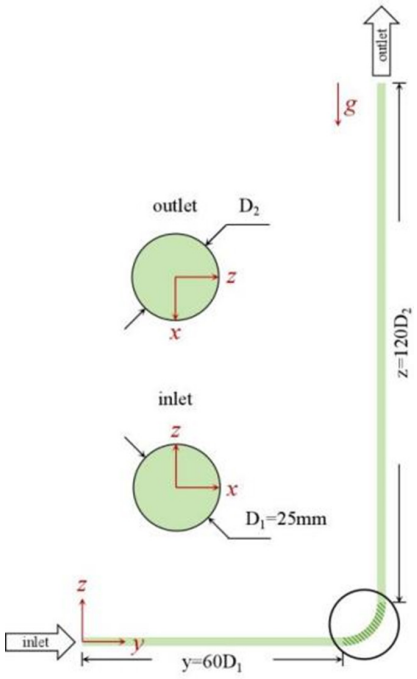

Figure 2: Geometric model principle diagram.

Meshing scheme: Figure 3 presents a schematic of the structured mesh for the elbow pipe. The inlet cross-section employs an O-type meshing method for the circular pipe cross-section to ensure mesh quality in the near-wall region. Considering stress concentration characteristics and complex flow phenomena (e.g., secondary flow) in the elbow area, localized mesh refinement was applied. As shown in Figure 3, the axial 3D meshing configuration for both the elbow region and inlet area effectively captures flow field details of gas-liquid two-phase flow during flow direction transition, achieving improved numerical simulation accuracy while maintaining computational efficiency (Figure 3).

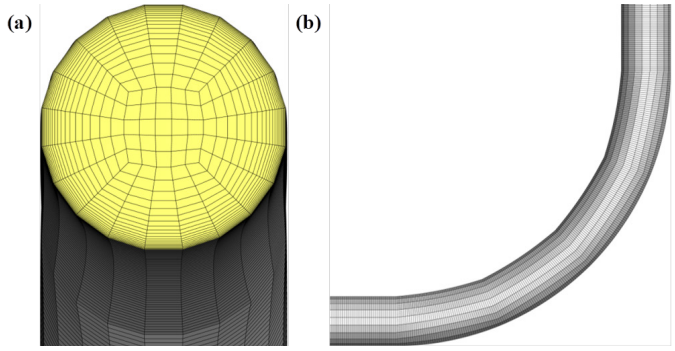

Figure 3: Structural mesh schematic diagram of 90-degree diameter circular elbow pipe: (a) inlet cross-section mesh; (b) axial three-dimensional mesh of elbow inlet region and elbow region.

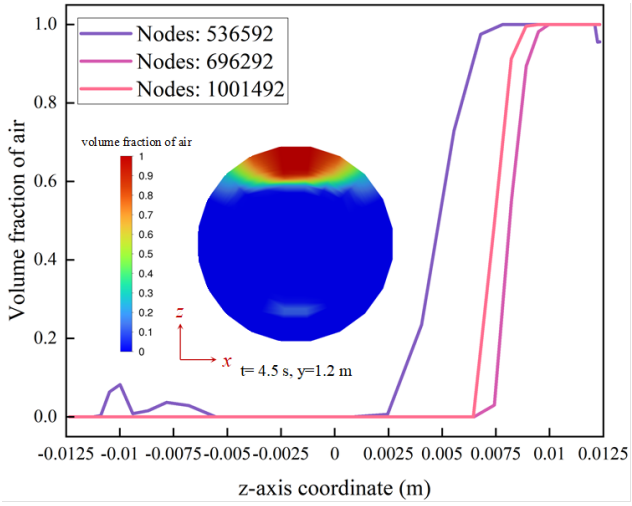

Figure 4: Distribution of gas phase volume fraction along z-axis position coordinates for different mesh numbers.

Mesh independence verification: This study conducted comparative analyses of three grid density configurations (536,592,696,292 and 1,001,492 mesh elements) for a 90-degree diameter circular elbow model. The primary focus was analyzing the radial gas-phase volume fraction distribution along the z-axis at the horizontal pipe section (y=1.2m) at time t=4.5s, as illustrated in Figure 4. Results demonstrated that all grid configurations effectively captured the stratified flow characteristics of gas-liquid two-phase systems, with liquid phase predominantly concentrated at the pipe base and gas phase accumulating at the top. Notably, when grid density increased from 536,592 to 696,292, the gas-phase volume fraction distribution curve exhibited significant changes, with the gas-liquid interface transition point shifting from z=0.00246431 to z=0.00684237. Further grid densification to 1,001,492 resulted in a more gradual curve transition with only minor displacement of the transition point (from z=0.00684237 to z=0.00645014). These findings indicate that computational stability is achieved at grid density 696,292, where additional density increments yield negligible impact on results. Therefore, adopting this grid configuration optimizes computational efficiency

while maintaining accuracy. Considering geometric similarity across circular pipe models with different connection structures, subsequent simulations uniformly adopted this grid scheme to ensure consistency and reliability throughout the research process (Figure 4).

Mathematical models and control equations

The flow of gas-liquid two-phase systems in pipelines constitutes an exceptionally complex physical process. Particularly when fluids pass through elbows, significant secondary flow phenomena occur accompanied by dynamic variations in critical parameters such as gas holdup. To investigate how horizontal-vertical pipe connection configurations influence phase distribution in two-phase flows, this study employs Ansys Fluent software for numerical simulations. The simulation requires maintaining clear phase interface delineation, accurately capturing phase interface evolution characteristics, and enabling effective flow pattern identification. After comprehensive evaluation, the k-ε model was selected for its superior simulation capabilities for complex flow phenomena including secondary flow, combined with the VOF model's advantages in multiphase interface tracking. This study selects the standard k-ε turbulence model, mainly due to its good simulation accuracy and computational robustness for complex turbulent phenomena in pipe flows, especially secondary flows in curved sections. This model is one of the most widely used RANS models in engineering and performs well in predicting turbulence with mean strain, with relatively low computational cost, making it suitable for simulating the macroscopic evolution characteristics of the horizontal-vertical transition flow field in this study. However, the standard k-ε model also has certain limitations. As a high Reynolds number model, its assumptions may no longer be fully applicable in the near-wall region (viscous sublayer and transition layer). This study relies on the wall function method to handle near-wall flows, which may affect the simulation accuracy of the fine structures of the gas-liquid interface in the near-wall region (such as extremely thin liquid films). Additionally, the model may have deviations in predicting certain details of strong swirling or separated flows. Consequently, the VOF (Volume of Fluid) multiphase flow model and standard k-ε turbulence model were adopted for numerical simulations.

The VOF model employs a unified momentum equation for solution and captures the dynamic evolution of phase interfaces between two or more immiscible fluids by continuously monitoring the volume fractions of each phase within the computational domain. In this study, the gas-liquid phase transition transfer process is not considered, and the governing equations include the mass conservation equation, momentum conservation equation, and turbulence equation.

The continuity equation is:

$$\frac{\partial}{\partial t}\left(\rho_i \alpha_i\right)+\nabla.\left(\rho_i \alpha_i v_i\right)=0$$

Where, i represents the gas phase (g) or liquid phase (l); ρ_i denotes the density of phase i; α_i indicates the volume fraction of phase i; and v_i signifies the velocity of phase i.

The momentum equation is:

$$\frac{\partial}{\partial t}\left(\rho_i \alpha_i v_i\right)+\nabla.\left(\rho_i \alpha_i v_i v_i\right)=-\alpha_i \nabla p+\nabla.\tau_i+\rho_i \alpha_i g+F_i$$

Where, τ_i denotes the stress tensor, while F_i represents the interfacial force between gas and liquid phases.

The standard k-ε model consists of the turbulent kinetic energy equation (k equation) and the turbulent dissipation rate equation (ε equation), with the following transport equations:

$$\frac{\partial}{\partial t}(\rho k)+\frac{\partial}{\partial x_i}(\rho k \mu_i)=\frac{\partial}{\partial x_j}\left[\frac{\partial k}{\partial x_j}\left(\mu+\frac{\mu_t}{\sigma_k}\right)\right]+G_k+G_b-\rho\varepsilon-Y_M+\varphi_k$$

$$\frac{\partial}{\partial t}(\rho\varepsilon)+\frac{\partial}{\partial x_i}(\rho\varepsilon\mu_i)=\frac{\partial}{\partial x_j}\left[\frac{\partial \varepsilon}{\partial x_j}\left(\mu+\frac{\mu_t}{\sigma_s}\right)\right]+\frac{C_{1s}}{k}(G_k+G_b C_{3s})-C_{2s}\rho\frac{\varepsilon^2}{k}+\varphi_s$$

Where, k denotes turbulent kinetic energy; ε represents the turbulent kinetic energy dissipation rate; x_i and x_j are coordinate components; μ_i is the viscosity coefficient component; μ_t is the turbulent viscosity coefficient; G_{-k} denotes turbulent kinetic energy induced by velocity gradients; G_b is the turbulent kinetic energy term caused by buoyancy; Y_M indicates the influence of compressible fluid turbulent pulsation expansion on the turbulent dissipation rate ε; with C_{1s} = 1.42 and C_{2s} = 1.68.

Boundary conditions and solution settings

Specify inlet conditions (U_{sg}=0.22 m/s, U_{sl}=0.46 m/s), pressure outlet and non-slip walls. Specify the solution algorithm (e.g., PISO).

To accurately simulate actual flow conditions, the numerical model comprehensively considers the effects of gravity, volumetric forces, and surface tension. A gravity field is established, with volumetric force equations and surface tension models selected. The working fluids involved are water and air, both of which are incompressible fluids with constant physical properties, and heat conduction is neglected. The solution method employs the Pressure Implicit Operator Splitting (PISO) method to handle the coupling between pressure and velocity fields. Two momentum correction indices were introduced to significantly enhance the convergence rate during transient calculations. The pressure equation is solved using the Pressure Interpolation Algorithm (PRESTO), while the volumetric fraction difference employs the Geometric Reconstruction scheme (Geo-Reconstruct). Relaxation factor terms and other parameters were set to default values in the software to ensure computational versatility and comparability. Boundary conditions and force parameters are specified as shown in (Table 1).

Table 1: Boundary conditions and force parameter setup.

Boundary Condition Term	Value
inlet	mixed-phase inlet velocity: 0.68m/s Gas phase volume fraction: 0.3235
outlet	free flow outlet
wall	non-sliding wall surface
initial time	filled with water
gravitational field	along the negative z-axis direction, gravitational acceleration g=9.81m/s^2
surface tension coefficient of water	0.072N/m

Model validation

To validate the effectiveness of the adopted CFD model, Figure 5 illustrates the distribution of liquid film thickness along Taylor bubble length in both numerical simulations and experimental data. The elastic bubble heads exhibit a semi-circular shape in both simulations and experiments, with consistent distribution of the gas-liquid interface (liquid film thickness η/D). These findings confirm the accuracy of the multiphase flow and turbulence models in the CFD simulation, demonstrating their capability to accurately capture the flow patterns of elastic flow and gas-liquid interface distribution within vertical riser systems (Figure 5).

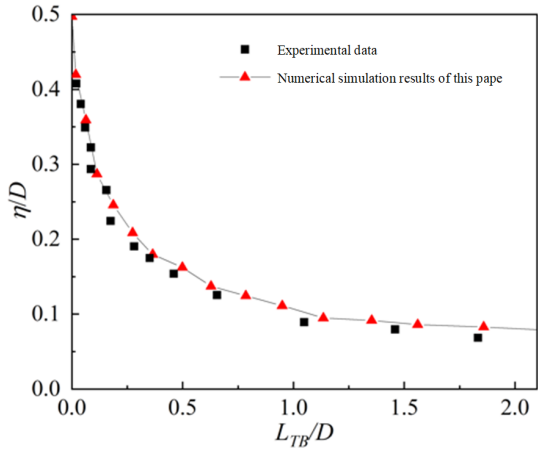

Figure 5: Distribution of liquid film thickness along bubble length in experimental results and numerical simulations.

Results and Discussion

To investigate the influence of horizontal-vertical pipe connection configurations on gas-liquid two-phase flow mixing characteristics, this section employs the numerical simulation methods described earlier. We conduct three-dimensional numerical simulations of gas-liquid two-phase flow in an equal-diameter circular bending pipe with an inner diameter of 25mm and curvature radius R=5D. Using the CFD-Post post-processing software system, we extract and analyze key flow field parameters including fluid phase distribution, velocity field, and pressure field to elucidate the evolution mechanisms of phase distribution during horizontal-to-vertical flow transition processes

Flow characteristics of gas-liquid two-phase flow

Evolution of gas-liquid two-phase flow patterns in horizontal and vertical tubes: In numerical simulation studies, the configuration of inlet boundary conditions critically influences the formation and development of two-phase flow patterns. This study employed an inlet condition with gas phase apparent velocity of 0.22m/s and liquid phase apparent velocity of 0.46m/s, as illustrated in (Figure 6).

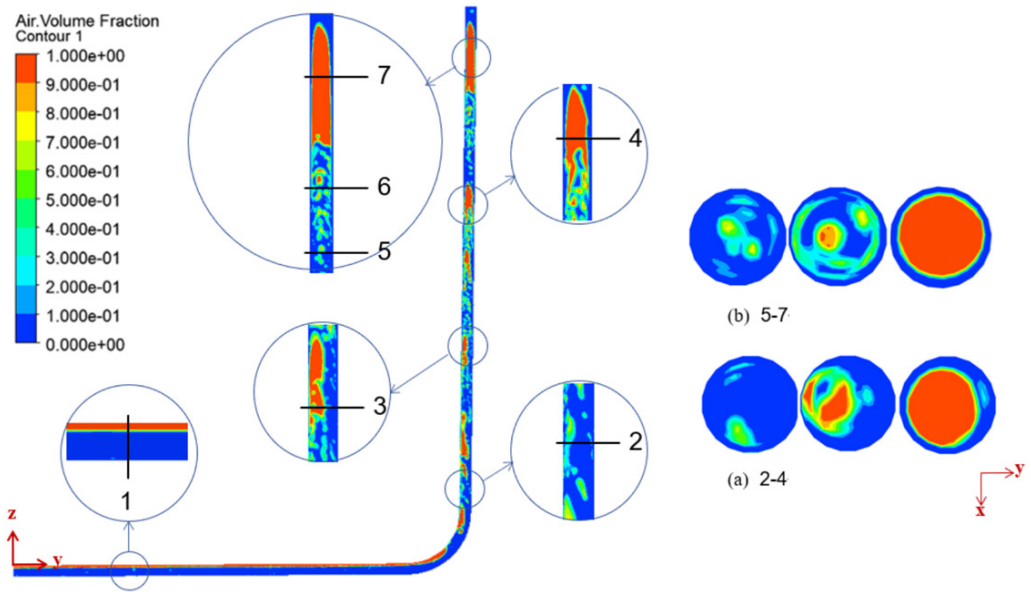

Figure 6: Development cloud map of gas phase volume fraction distribution in the curved pipe.

Under fully developed flow conditions, horizontal pipe sections exhibit typical two-phase stratified flow characteristics of gas and liquid. Analysis of the gas volume fraction distribution cloud map (Figure 4) reveals a distinct radial gradient along the z-axis in the horizontal pipe cross-section at position 1: the gas volume fraction exceeds 0.9 in the upper pipe region while remaining below 0.1 in the lower section. This distribution pattern indicates that under gravitational forces, the gas phase predominantly flows in the upper section of the horizontal pipe, whereas the liquid phase moves along the lower section, forming a clear and stable interfacial boundary between the two phases.

When the fluid flows through the 90-degree elbow into the vertical pipe section, the flow pattern of the gas-liquid two-phase flow evolves into a slug flow characterized by alternating Taylor bubbles and liquid plugs due to enhanced buoyancy forces and directional changes. Systematic analysis of the gas phase volume fraction distribution cloud maps at cross-sections 2-7 of the vertical pipe (Figure 6) clearly demonstrates the phase distribution evolution: In the bottom region adjacent to the elbow outlet (position 2), the average gas phase volume fraction significantly drops below 0.1, indicating the formation of stable liquid plug structures. These structures not only disrupt continuous gas distribution at the pipe base but also create essential conditions for subsequent Taylor bubble generation. As the flow progresses upward to position 3, it enters a transitional zone where residual centrifugal effects combined with buoyancy forces drive gas phase migration from the initial inner elbow region toward the pipe center, accompanied by significant gas-liquid interface instability and mixing phenomena. By position 4, buoyancy becomes dominant, resulting in the formation of characteristic gas core structures within the central pipe region.

Furthermore, the low gas phase fraction zone near the height of position 5 in the cloud map corresponds to the liquid plug region in the bullet flow regime. At position 7, a typical Taylor bubble structure can be observed: a gas core region with diameter-scale gas phase (volume fraction approaching 1.0) forms at the pipe center, exhibiting a conical bubble head and flattened tail resembling bullet-shaped morphology. Near the wall region maintains sub-0.1 gas phase volume fraction, creating distinct annular liquid film structures. Notably, complex gas-liquid mixing phenomena emerge at the Taylor bubble tail region (position 6), where vortex-like mixing zones appear in the vertical pipe cross-section phase distribution cloud map. The gas-liquid interface demonstrates significant instability characteristics with markedly reduced clarity compared to the bubble head region. This series of phase distribution evolution processes fully demonstrates the critical impact of horizontal-vertical flow direction transition on gas-liquid two-phase flow characteristics.

Gas-liquid flow characteristics in bend region: As the developed laminar flow in the horizontal pipe enters the 90-degree elbow region, centrifugal force deflects the heavy liquid phase outward, forming a continuous and stable liquid film. Meanwhile, the low-density gas phase is compressed inward and gradually accumulates, creating a high-volume fraction gas cluster at the elbow inlet. The gas flow channel narrows at the corner apex, as illustrated in Figure 7a gas volume fraction cloud diagram. During fluid discharge from the elbow, newly separated gas clusters from the continuous gas phase in the horizontal pipe ascend along the inner wall surface driven by buoyancy and flow drag force, exhibiting a skewed distribution in the vertical pipe section. The liquid film on the outer elbow side refills the outlet, forming a liquid plug that separates adjacent gas clusters. This process represents the initial evolution from laminar flow to slug flow: alternating occurrences of gas clusters, liquid plugs, and gas clusters constitute the characteristic slug flow cycle (Figure 7).

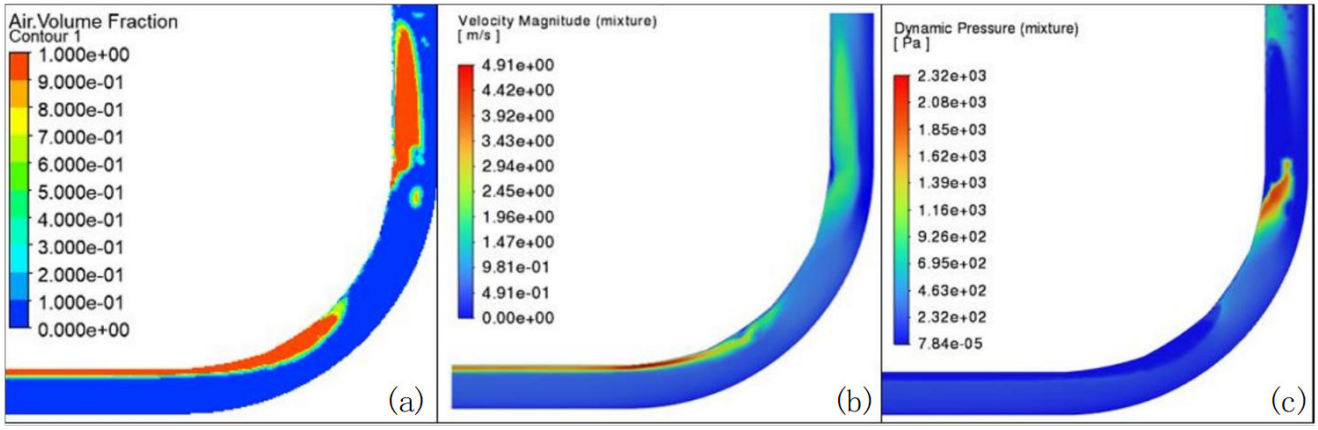

Figure 7: Flow development cloud diagram of gas-liquid two-phase flow in a curved pipe: (a) Gas volume fraction cloud diagram; (b) Velocity cloud diagram; (c) Dynamic pressure cloud diagram

Figure 7b-c illustrates the mechanism of rising bubble formation and detachment through velocity field analysis and dynamic pressure cloud mapping: The liquid phase region adjacent to the tail of detached bubbles exhibits dynamic pressure peaks ($\approx 2.3\times10^3$Pa) and pressure differentials caused by low-pressure troughs in the liquid film outside the elbow. This pressure gradient impedes gas-phase flow, preventing direct penetration through the outer liquid film into the vertical section. Consequently, bubbles

accumulate at elbow corners, disrupting stratified flow continuity in horizontal pipes. Within horizontal stratified flows, gas-phase particles experience accelerated motion due to flow channel constriction at elbow entrances and viscous drag forces, with local velocities reaching 4.9m/s. Concurrently, liquid film narrowing caused by bubble aggregation increases flow velocity at these zones, generating intense viscous resistance at gas-liquid interfaces. Combined with surface tension effects, this induces "necking" at critical thickness levels where bubbles detach as discrete units rather than sliding as a continuum. Detached bubbles ascend along vertical pipe sections propelled by buoyancy and incoming flow, while liquid films rapidly recombine into plug formations at elbow outlets to isolate adjacent bubbles. This process establishes elastic flow structures in subsequent pipe sections, demonstrating phase distribution evolution from horizontal stratified flow to vertical elastic flow. The flow dynamics clearly reveal the kinematic characteristics of gas-phase aggregation and plug-mediated separation at elbow junctions.

Dynamic evolution patterns of gas-liquid interfaces in bend regions: After a period of numerical simulation calculations, the gas-liquid two-phase flow has reached a relatively stable state. The average cycle time for bubble formation and detachment in the elbow region is 0.1 seconds. A representative gas-liquid two-phase distribution diagram (Figure 8) was selected within this timeframe to analyze how the geometric configuration of conventional 90-degree equal-diameter elbows influences the formation and development of slug flow bubbles (Figure 8).

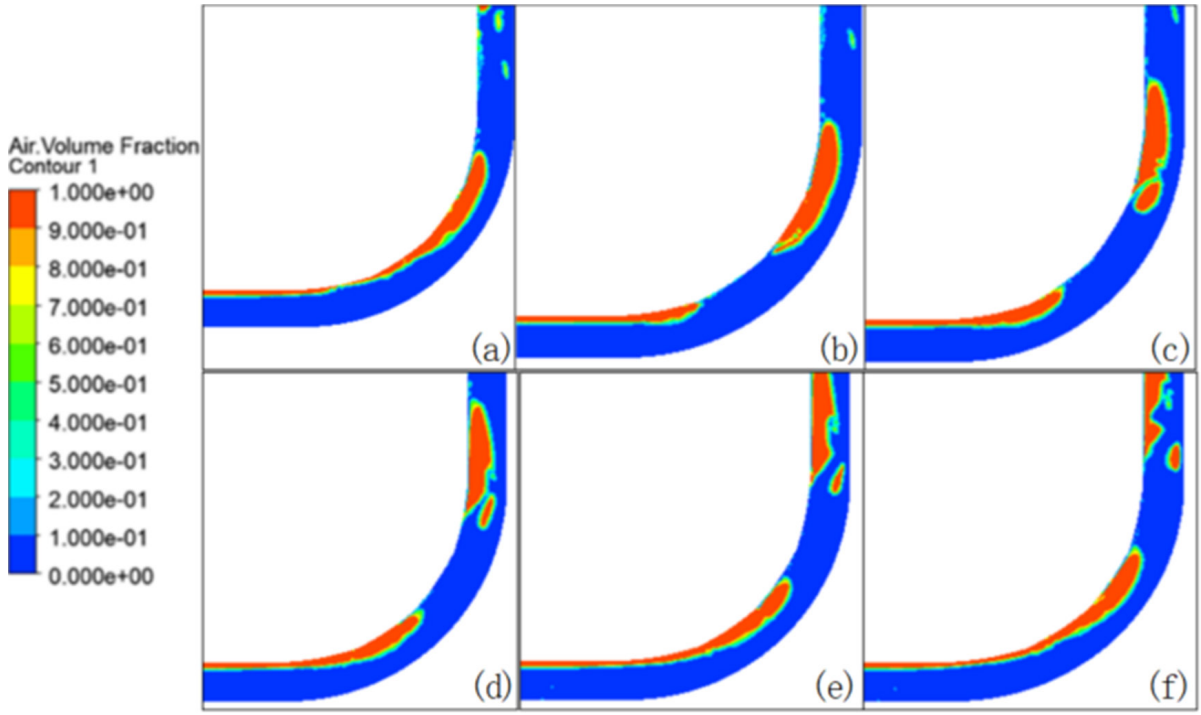

Figure 8: Evolution of gas-liquid phase distribution in the elbow region during a single bubble generation cycle: (a) 10.55s; (b) 10.57s; (c) 10.60s; (d) 10.63s; (e) 10.65s; (f) 10.67s.

The Figure 8 illustrates the second bubble nucleation-necking-detachment process and residual gas film re-agglomeration at the elbow bottom, following the initial bubble's imminent detachment at 10.55 seconds. Starting from this time point, the tail of the agglomerated gas mass contracts to its limit, preparing to separate from the continuous gas phase in the horizontal pipe and detach into a bubble. Meanwhile, the residual gas film remains adhered to the top wall of the horizontal pipe while advancing forward along the inner side of the elbow.

At 10.57 seconds, continuous replenishment of horizontal incoming gas phase caused the gas film at the elbow inlet to progressively thicken and coalesce, forming the initial "bulge" of the next bubble. From 10.60 to 10.63 seconds, gas phase continued coalescing, sliding continuously along the inner wall of the elbow and extending toward the vertical pipe. By 10.65 seconds, the gas film neck underwent significant contraction under combined effects of interfacial tension and liquid viscous drag force, gradually separating from the coalescing gas mass. By 10.67 seconds, neck contraction was complete: the second intact bubble detached from the continuous gas film and rose upward via buoyancy, while residual gas film at the elbow base re-coalesced, preparing for subsequent cycles. Throughout this process, the abrupt curvature of the 90-degree equal-diameter elbow intensified centrifugal separation effects, accelerating gas phase accumulation and coalescence on the inner wall. Concurrently, flow direction changes amplified stress concentration at the gas-liquid interface, hastening gas film accumulation and neck contraction while determining bubble detachment timing and size-critical factors influencing the generation frequency and characteristic dimensions of elastic flow plugs.

Criterion for full development of elastoclastic flow in vertical pipe sections

After conducting numerical simulations over a specified duration, comparative analysis of gas-phase volume distribution cloud diagrams at different time points revealed that in conventional 90-degree equal-diameter elbow pipes, Taylor bubbles in the elastic flow had reached full development at a height of 2.24465m (89.8D) within the vertical pipe at 7.2 seconds (as shown in Figure 9). At this stage, the Taylor bubbles 'diameter approached the pipe's inner diameter, forming a flow structure resembling blockage. The bubble heads exhibited rounded and plump shapes, while the tail-phase interfaces remained nearly flat. No further bubble coalescence occurred during subsequent flow processes (Figure 9).

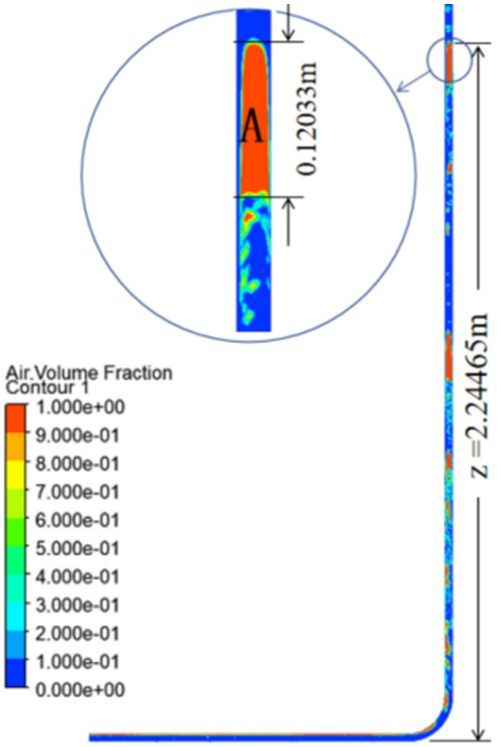

Figure 9: Cloud map of fully developed ellipsoidal flow gas phase volume fraction distribution

Using gas-phase apparent velocity of 0.22m/s and liquid-phase apparent velocity of 0.46m/s as inlet conditions, empirical formulas (Equations 2-4) indicate that when the slug flow in the vertical tube reaches fully developed state, the Taylor bubble rising velocity UTB=0.98925m/s. This value can serve as a criterion for determining whether slug flow has achieved full development in the numerical simulation studies presented herein.

Since the upward velocity of Taylor bubbles cannot be directly derived from numerical simulation results at a specific time point, their vertical velocity in the pipe must be calculated by determining the difference between the z-axis heights of the same Taylor bubble at two adjacent time intervals and applying a time factor. Therefore, a Taylor bubble at a height of 2.24465m was selected as the study subject. By processing the z-axis coordinate data of the bubble's tip at three time points (7.17s, 7.20s, and 7.23s), the upward velocity at 7.20s was calculated to be 1.0222m/s, showing a computational error of approximately 3.33% compared to the theoretical fully developed state velocity UTB. Considering unavoidable errors such as mesh resolution limitations and sampling point offset, this error remains within an acceptable range of <5%. Thus, it can be concluded that the slug flow at the 2.24465m height (89.8D) has reached the fully developed state (Figure 10).

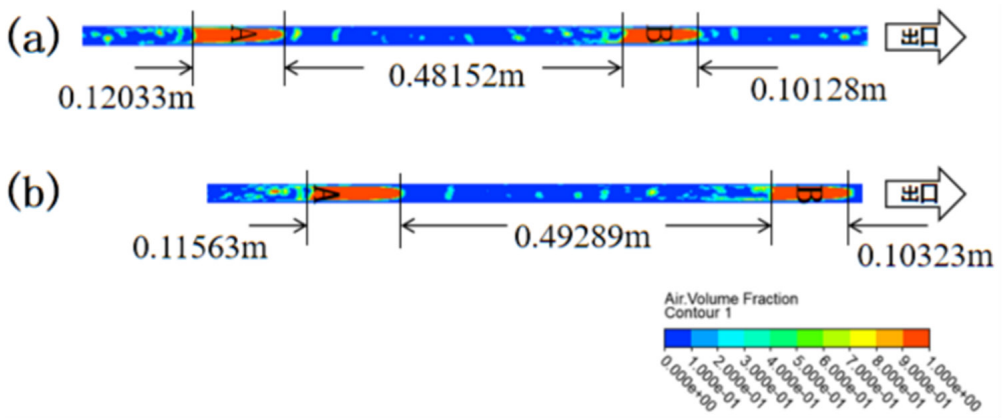

Figure 10: Cloud maps of elastic flow gas phase volume fraction distribution near the outlet region of vertical pipe sections at two time points: (a) 7.2s; (b) 7.4s

At 7.2 seconds, the Taylor bubble A at a height of 2.24465m (89.8D) shown in Figure10a had a length of 0.12033m. The liquid plug length between this bubble and the adjacent Taylor bubble B at 2.83055m height was 0.48152m (19.26D), while bubble B itself measured 0.10128m in length. By 7.4 seconds, the original upper bubble B was about to exit the vertical pipe outlet (as shown in Figure 10b). At this stage, the bubble lengths of the original lower bubble A and upper bubble B were 0.11563 m and 0.10323 m respectively, showing relative errors of approximately 3.91% and 1.93% compared to 7.2 seconds measurements. The liquid plug length between the two bubbles remained at 0.49289 m, with a relative error of about 1.64% from 7.2 seconds values-all within acceptable limits below 5%. These findings indicate that the movement velocities between different Taylor bubbles and between liquid plugs are approximately equal, with both length and phase interface distribution reaching full development, thereby achieving stable flow patterns.

The analysis indicates that in conventional 90-degree diameter elbow pipes, the minimum pipe length required for Taylor bubble development in vertical pipes is 2.11965 meters (approximately 84.8D). It should be emphasized that this minimum development length of approximately 85 days is the simulation result under the specific conditions of the pipe inner diameter (D=25mm), elbow curvature radius (R=5D), and apparent inlet velocity (U_sg=0.22m/s, U_sl=0.46m/s) in this study. Different system geometric parameters (such as pipe diameter, elbow curvature ratio) and operating conditions (such as gas-liquid flow rate, physical properties) may have a significant impact on the development length of the elastic flow.

Conclusion

This study employs a three-dimensional numerical simulation method to investigate the phase distribution evolution mechanism of gas-liquid two-phase slug flow during the transition from horizontal to vertical upward flow in a conventional 90-degree equal-diameter elbow. The investigation focuses on the process of slug flow formation, development, and the minimum vertical pipe length required to achieve a fully developed state.

The main conclusions are as follows:

Under the combined action of centrifugal force, viscous drag, and surface tension within the elbow region, the initially stratified flow in the horizontal pipe undergoes a distinct "nucleation-necking-detachment" process, forming discrete gas bubbles. The liquid film on the outer wall of the elbow recombines to form liquid plugs, thereby initiating the transition to slug flow in the vertical pipe section. The dynamic evolution of the gas-liquid interface confirms that the geometric configuration of the bend significantly affects the frequency and dimensions of bubble detachment, which are key factors influencing slug flow development.

The slug flow is considered fully developed when the Taylor bubble in the vertical pipe exhibits a stable bullet shape with a conical head and flattened tail, and its diameter approaches the inner diameter of the pipe. At this stage, the rising velocity of the Taylor bubble, bubble length, and the length of the adjacent liquid plug all stabilize. The computed bubble rising velocity (1.0222m/s) is in close agreement with the theoretical value (0.98925m/s) based on empirical correlations, with an error of approximately 3.33%, validating the simulation's accuracy.

For the simulated configuration with a 25mm pipe inner diameter (D) and elbow curvature radius of 5D, under the simulated configuration (pipe inner diameter D=25mm, elbow curvature radius R=5D, and the specified inlet conditions), the minimum length required for the slug flow to achieve full development in the vertical pipe section is approximately 84.8D(2.12m). This indicates that under the conditions set in this study, at least about 85 times the pipe diameter of straight pipe section is required downstream of the conventional 90-degree equal-diameter elbow to achieve a stable and fully developed slug flow. This indicates that downstream of a conventional 90-degree elbow, a straight vertical pipe segment of at least 85 times the pipe diameter is necessary to ensure stable, fully developed slug flow conditions, which is crucial for the accurate application of flow measurement techniques (e.g., thermal diffusivity methods) that rely on such flow conditions.

The findings provide a theoretical basis for optimizing the layout of pipeline systems involving flow direction changes. To

reduce the space requirements and enhance system compactness in industrial applications (e.g., oil and gas wellheads), future research could explore alternative connection structures (e.g., varying bend angles, curvature radii, or streamlined transitions) that may promote more rapid slug flow development, thereby shortening the necessary development length. The validated numerical model serves as a reliable tool for such parametric studies.

References

1. Xu F, Li Y, Xu X, Yang J, Xiao F, et al. (2025) Thermal-hydrological-mechanical coupling simulation of matrix-type shale oil: Analysis of oil-gas-water multiphase flow mechanism under various parameter conditions. Geoenergy Science and Engineering 246: 213656.
2. Drury R, Hunt A, Brusey J (2019) Identification of horizontal slug flow structures for application in selective cross-correlation metering. Flow Measurement and Instrumentation 66: 141-149.
3. Fan Z, Zeng Q, Huang Y, Yuan B, Wei M, et al. (2026) A review of gas-liquid two-phase flow measurement: Sensing technologies and intelligent data analysis methods. Applied Thermal Engineering 284: 129173.
4. Liang F, Duan B, Li C, Zheng W, Zhu Y, et al. (2025) Gas-liquid two-phase flow rate measurement with differential pressure and density ratio synergistic dual neural network. Flow Measurement and Instrumentation 106: 102994.
5. Shakarami R, Sadeghi MT (2025) Gas-liquid two-phase flow measurement based on emitted acoustic signal anomaly and deep learning approach. Flow Measurement and Instrumentation p. 103097.
6. Zhang Z, Li Y, Wang Z, Hu Q, Wang D (2020) Experimental study on radial evolution of droplets in vertical gas-liquid two-phase annular flow. International Journal of Multiphase Flow 129: 103325.
7. Hu C, Liu Y, Yu M (2025) Influence of froude number on the development and evolution of secondary flows in a sharply curved bend: An experimental and numerical study. Advances in Water Resources 206: 105126.
8. Saidj F, Hasan A, Bouyahiaoui H, Zeghloul A, Azzi A (2018) Experimental study of the characteristics of an upward two-phase slug flow in a vertical pipe. Progress in Nuclear Energy 108: 428-437.
9. Babin V, Shemer L, Barnea D (2015) Local instantaneous heat transfer around a rising single Taylor bubble. International Journal of Heat and Mass Transfer 89: 884-893.
10. Talvy CA, Shemer L, Barnea D (2000) On the interaction between two consecutive elongated bubbles in a vertical pipe. International Journal of Multiphase Flow 26(12): 1905-1923.
11. Szalinski L, Abdulkareem LA, Silva MJD, Thiele S, Beyer M, et al. (2010) Comparative study of gas-oil and gas-water two-phase flow in a vertical pipe. Chemical Engineering Science 65(12): 3836-3848.
12. Hsu LC, Chen IY, Chyu CM, Wang CC (2015) Two-phase pressure drops and flow pattern observations in 90° bends subject to upward, downward and horizontal arrangements. Experimental Thermal and Fluid Science 68: 484-492.
13. Han F, Ong MC, Xing Y, Li W (2020) Three-dimensional numerical investigation of laminar flow in blind-tee pipes. Ocean Engineering 217: 107962.